Invited Paper

Spectral Ellipsometry of Semiconductors and Semiconductor Structures

L. Viña, M. Garriga+ and M. Cardona+

Instituto de Ciencia de Materiales C.S.I.C., and Departamento de Fisica Aplicada C-IV. Universidad Autónoma. 28049 Madrid. SPAIN

+Max-Planck Institut für Festkörperforschung. Heisenbergstrasse 1, 7000 Stuttgart 80. F.R.G.

ABSTRACT

Spectral ellipsometry has been proven to be a very powerful tool to study the band structure and electronic properties of semiconductors. Line-shape analysis of the derivative spectra of the pseudo-dielectric function allows a precise determination of critical point parameters, such as amplitudes, energies, broadening and excitonic phase angles. Here we will review the application of the technique, showing examples of the effects of temperature, alloy and doping in the band structure of semiconductors and the effects of a new periodicity along the growth direction in semiconductor structures.

1. INTRODUCTION

Spectral ellipsometry provides a precise and direct measure of the real and imaginary parts of the dielectric function for bulk materials and thin films. The technique has been widely used to determine the optical constants of solids in the NIR-VIS-NUV spectral region. It is based on the measurement of the change of the state of polarization of the light after reflection on a sample.[1] Generally, a linearly polarized light, incident at an oblique angle on the sample, will be elliptically polarized after reflection. Measuring the orientation of the ellipse and its ellipticity, or the related angles,[2] Ψ and Δ, one obtains the complex Fresnel reflection coefficients With the use of an appropriate model (usually a two- or three-phase model), the complex dielectric function is obtained. Typical systems consist of a collimated, unpolarized, monochromatic light-source, a polarizer, a compensator, a reflecting surface, an analyzer and a detector.

The rotating-analyzer technique,[3-4] based on a development by Aspnes, is ideal for spectroscopic studies due to its achromaticity (this configuration does not use a compensator), can be easily automated, has a high speed of data collection and high accuracy. The precision of the data obtained with automatic spectro-ellipsometry is such that derivative spectra can be obtained numerically and thus the parameters of interband critical points (CP's) can be found very accurately. The method has the advantage, with respect to modulation spectroscopy techniques, that the effect of external parameters, such as an electric field in electroreflectance, does not enter, therefore facilitating the interpretation of the data.

In order to obtain reliable values for the dielectric function (ϵ) is necessary to perform adequate surface treatments (lapping and polishing, chemical etching and rinsing) so as to remove unwanted surface layers. The goodness of a surface preparation can be checked by the usual criterion that the values of the imaginary part of ϵ be maximized in the ultraviolet region[5] (in zinc-blende-type materials around the E_2 gap). A three-phase model allows one to correct for thin overlayers, such as those produced by oxidation, and thus to extract the ϵ of the bulk material under study.

The dependence of critical point parameters on temperature and other perturbations such as heavy doping with donors and acceptors has been investigated systematically in the last years. Calculations of the changes of the CP's have been performed based on realistic band structures and lattice dynamics.[6-8] The experimental method is also very useful to study anisotropic systems such as CdSe,[9] and even biaxial ones such as GeS.[10] Short-period superlattices (SL's) are new, manmade crystals with physical properties different from those of their parent compounds. Their optical properties are influenced by the new periodicity along the SL growth direction. Its effects on the fundamental band gap have been extensively studied in the literature.[11] These studies are, however, scarcer for the higher interband transitions.[12-16]

The spectral range of spectro-ellipsometry has been recently extended beyond the range of conventional ellipsometry, up to 35eV, using synchrotron radiation light and triple-reflection polarizers.[17] This energy range can be used to investigate the band structure of wide band-gap semiconductors and insulators and to study excitonic structures arising from transitions from shallow core-levels.

This paper will deal with the determination of critical point parameters by means of spectro-ellipsometry. In the first section the effects of temperature will be presented. Next a discussion of those of heavy-doping will be given. A section on alloy effects will follow. Examples of anisotropic systems are also shown. The following section deals with microstructures. Finally some results for high T_c superconductors and ellipsometry in the UV will be reviewed.

2. TEMPERATURE DEPENDENCE OF CRITICAL POINTS

Investigations of the temperature dependence of the optical properties of semiconductors are of great importance, both from a theoretical and an applied point of view. The temperature can be used as an external parameter to change the band structure of the material. A precise determination of the changes of the optical constants of semiconductors with temperature is of crucial importance for the development of solar cells and other devices and for the understanding of laser-annealing processes.[18,19] For calculations of the temperature dependence of CP energies, both the effect of thermal expansion and electron-phonon interaction has to be taken into account. The latter effect must include Debye-Waller as well as self-energy terms.[20]

These temperature effects have been studied for a variety of semiconductors: germanium,[21,22] α-Sn,[23] InSb,[24] CdSe,[9] GaAs,[25,26] and silicon.[22,27] As an example we will show the effects for Ge.[21] Figure 1 shows the imaginary part of the dielectric function (ϵ_2) at four selected temperatures. The four main structures (E_1, $E_1+\Delta_1$, E'_0 and E_2 shift to lower energies and broaden with increasing temperature. The peaks in ϵ_2 corresponding to the E_1 and $E_1+\Delta_1$ CP's merge into a broad one, and an overall decrease of ϵ_2 with increasing temperature is also observed.

In order to enhance the structure in the spectra and to obtain the CP parameters, the second-derivative spectra are calculated numerically from the ellipsometric data. Figure 2 depicts the derivatives for ϵ_1 and ϵ_2. The lines show least-squares fittings to one-electron CP line shapes, where excitonic effects were taken into account by allowing mixture of two contiguous CP's.[28] The solid lines correspond to a mixture of a two-dimensional minimum and a saddle point which can be represented by[22]

$$\epsilon \sim C - \ln(E - \omega - i\Gamma)\, e^{i\phi} \qquad (1)$$

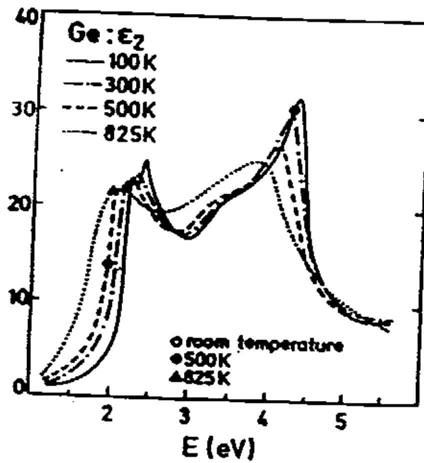

Figure 1.- Imaginary part of the dielectric function of germanium at different temperatures.

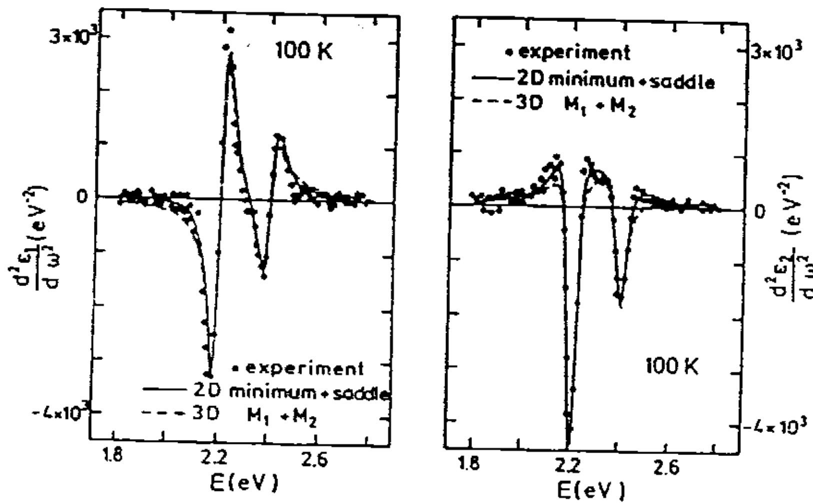

Figure 2.- Second-derivative spectra of the real and imaginary parts of the dielectric function of germanium at 100K. The lines represent fits of the critical points using standard line shapes and allowing excitonic interaction.

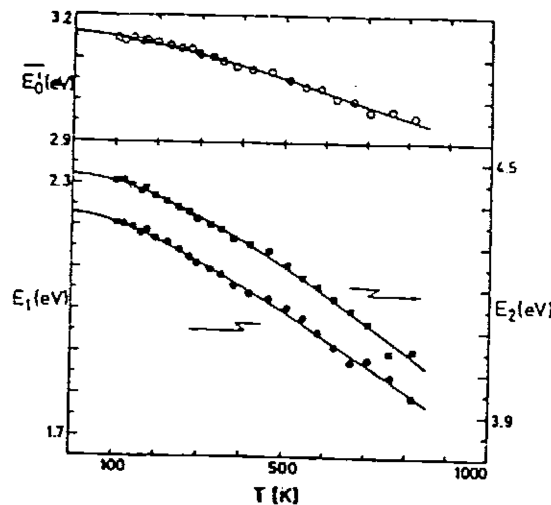

Figure 3.- Energy versus temperature of different critical points of Ge.

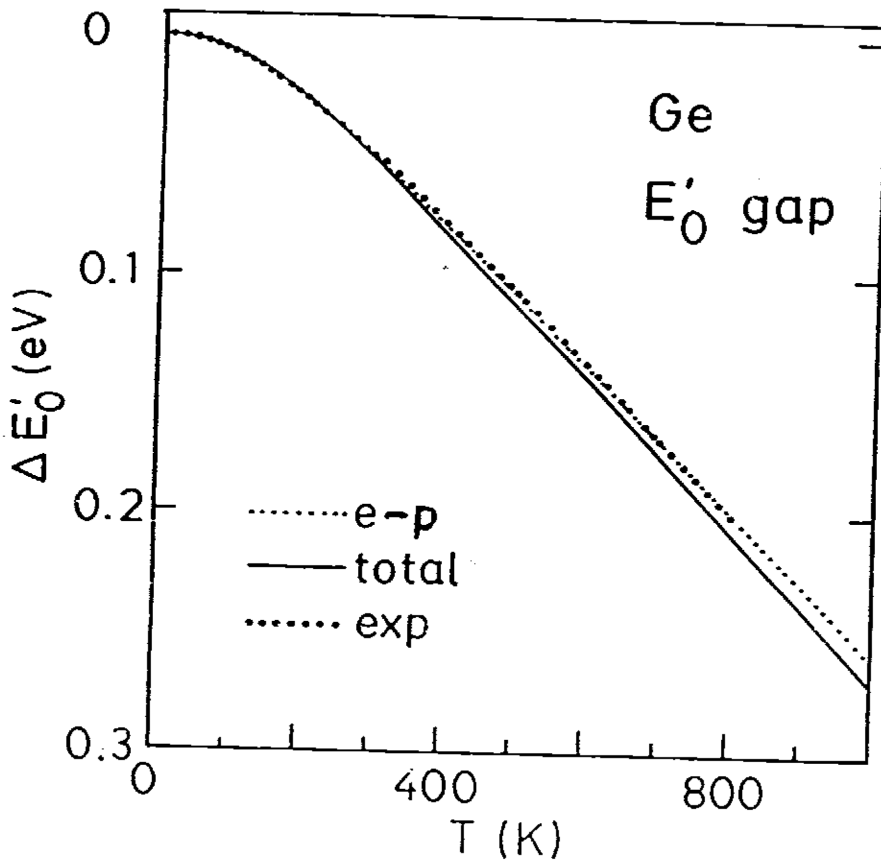

Figure 4.- Comparison of the experimental shift of the E'_0 of germanium versus temperature with results of theoretical calculations, after Ref. 22.

with the angle ø giving the amount of mixture. E is the critical point energy and Γ the broadening parameter.

Figure 3 shows the energy position of the E_1, E_2 and E'_0 CP's as a function of temperature. The results show a linear dependence of the gaps at high temperature and a quadratic one at low temperature. The solid lines correspond to the best fit with Varshni's empirical formula:[29]

$$E = a - \alpha T^2 / (\beta + T) \qquad (2)$$

The data can also be fitted to an expression where the energies decrease proportional to Bose-Einstein statistical factors for phonon emission plus absorption:

$$E = a - b\left[1 + 2 / (e^{\Theta/T} - 1)\right] \qquad (3)$$

The parameter Θ represents a mean temperature of the phonons taking part in the scattering process. A value of 360K (±120K) was obtained for the E_1 CP. Its large value indicates that acoustic phonons tend to contribute less than the optical ones at high temperatures, a fact reproduced by the calculations of temperature dependence of the gaps.[20,22] Figure 4 shows a comparison of the experimental shift for the E'_0 gap with the results of the theoretical calculations, including electron-phonon interaction (dotted lines) and the total effect (electron-phonon plus thermal expansion).[7]

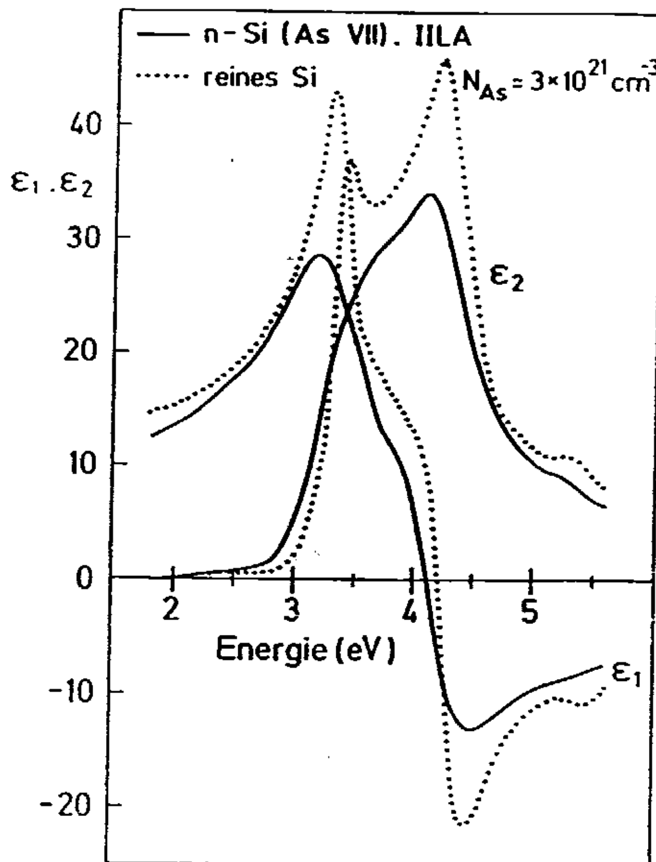

Figure 5.- Dielectric function of pure Si (dotted line) and an As-implanted laser annealed Si, with an As concentration of $3x10^{21}cm^{-3}$ (solid line).

3. HEAVY DOPING EFFECTS ON THE BAND STRUCTURE

The interest on heavy doping on semiconductors has grown in the last years, since high levels of doping allow further miniaturization of electronic devices and influence strongly their characteristics and performance. From a fundamental point of view, it is also important to study the optical spectra of disordered systems and to compare them with theoretical predictions of the changes of the band structure with impurity concentration. These effects have been studied for the higher band gaps mainly for Si[6,30,31] and germanium,[8] although most of the work concentrates on the fundamental band gap.[32] Due to its technological importance we present here results for ion-implanted, laser annealed (IILA) and bulk-doped Si, with an impurity concentration ranging from $N>10^{13}cm^{-3}$ to $N\sim 3x10^{21}cm^{-3}$. Both n- and p-type samples were studied.[6] Similar experiments were also performed for Ge.[8]

The dielectric function for an As-implanted, laser annealed Si is shown in Fig. 5. The dotted lines represent ϵ of undoped Si. A large red-shift and lifetime broadening of the E_1 (~3.4eV) and E_2(~4.25eV) CP's is observed for the implanted sample. The contributions of free carriers is only important in the lower part of the spectrum (energies below ~2.5 eV) and can be neglected at the energies where E_1 and E_2 occur. One of the most dramatic effects of the doping is the blurring of the E_1 peak, which becomes a shoulder for high doping concentrations. This has been attributed to a decrease of the excitonic interaction in the E_1 CP due to the screening of free carriers.[6]

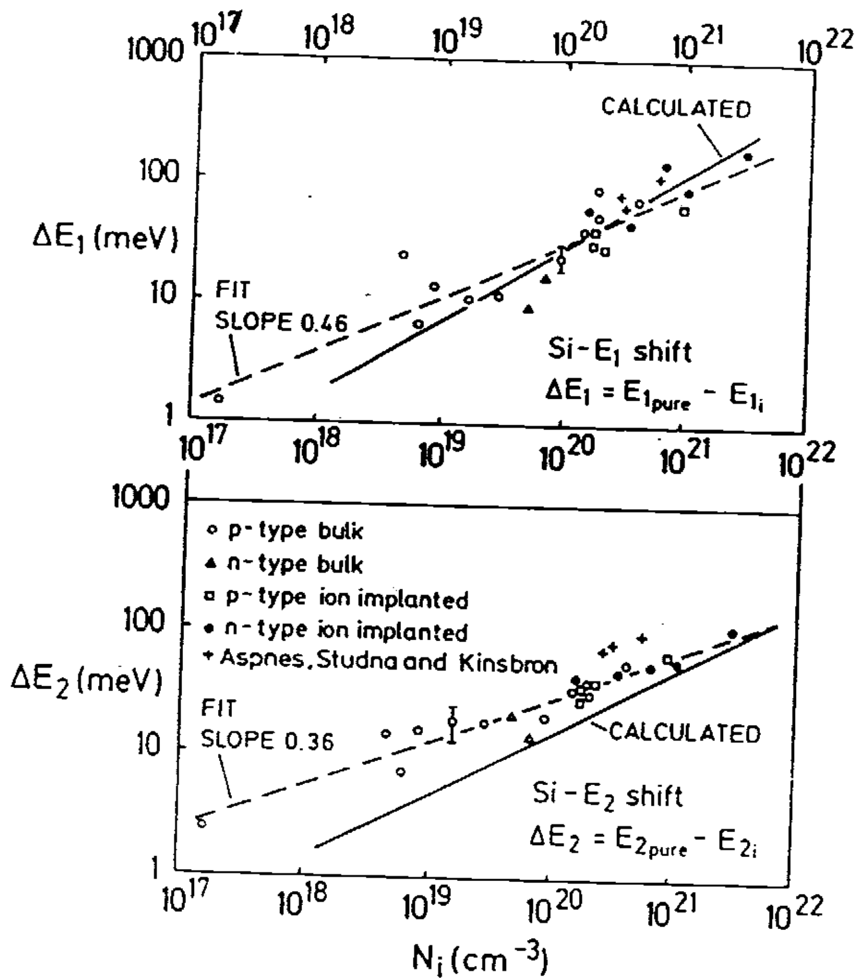

Figure 6.- Energy shift versus carrier concentration of the E_1 and E_2 CP's of Si. Dashed lines are fits to a power law. Solid lines are results of calculations after Ref. 6.

The shifts of the critical points with doping are shown in Fig. 6. No systematic differences were observed between p- and n-type doping. The effects of doping become noticeable above 10^{19}cm^{-3}. The dashed lines show the best fit to a power law. The solid lines are the results of a pseudopotential band structure calculation for the self energies of the CP's in perturbation-theory up to second-order. The main effects arise from the second-order terms, the first-order perturbation shifts are negligible except for $N>10^{21}$ cm^{-3}. This also agree with the experimental finding that the shifts and broadenings do not depend on the nature of the dopant (n- versus p-type).

4. OPTICAL CONSTANTS OF ALLOYS AND ANISOTROPIC SEMICONDUCTORS

We will concentrate on the optical properties of II-VI alloys. They can be considered as an additional class of II-VI compounds, where the different band structure parameters may be continuously varied (virtual crystal approximation). This allows the tuning of the optical band gap between those of their parent compounds, and to optimize optical devices such as injection lasers and infrared detectors. The systems $Cd_xHg_{1-x}Te$,[33] $Zn_xHg_{1-x}Se$,[34] $Cd_xHg_{1-x}Se$[35] and $Cd_{1-x}Mn_xTe$[36] have been studied.

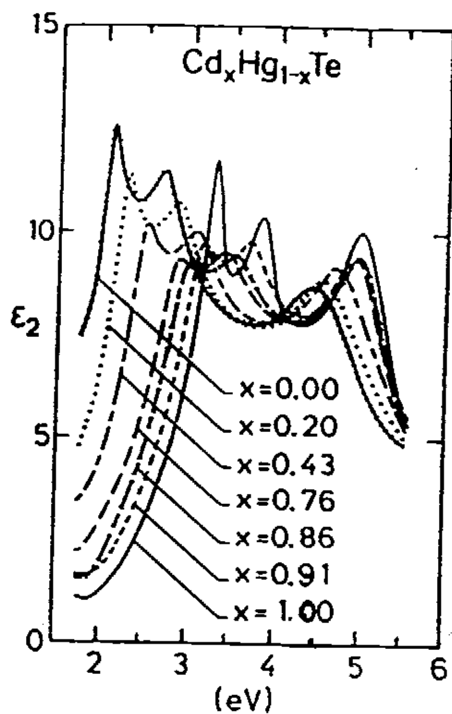

Figure 7.- Imaginary part of the dielectric function of $Cd_xHg_{1-x}Te$ for different alloy compositions.

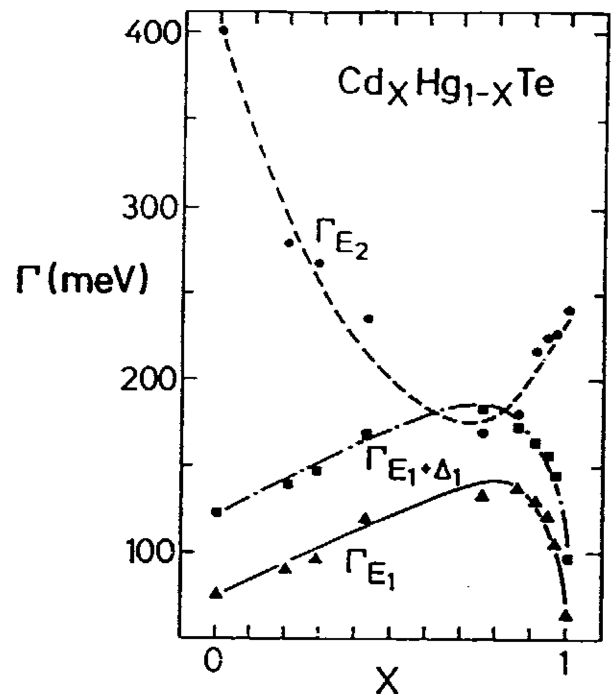

Figure 8.- Dependence on x of the broadening parameter of the E_1, $E_1+\Delta_1$ and E_2 CP's of $Cd_xHg_{1-x}Te$ for different alloy compositions.

$Cd_xHg_{1-x}Te$ is a mixture of a semimetal (HgTe) with a semiconductor (CdTe), crystallizing in the zinc-blende structure. It has attracted considerably attention due to its application as infrared detector. The main effect of alloying in the fundamental band gap is the quadratic dependence of the energy thresholds on composition x. For higher gaps the magnitude and even the sign of the bowing relative to the fundamental edge can change. Lifetime broadening effects are also present in higher gaps.[33,37] Another effect which is mainly disorder induced is the nonlinear dependence of spin-orbit splitting on alloy composition.[38] Figure 7 shows the imaginary part of the dielectric function for HgTe, CdTe and 5 different alloy compositions. The most important fact in this figure is the shift of the three main peaks (E_1, $E_1+\Delta_1$ and E_2) to higher energies with increasing x. A decrease of the magnitude of ϵ_2 happens until concentrations of ~0.7. The excitonic effect near the E_1 and $E_1+\Delta_1$ CP is also seen in the figure: the peaks in ϵ_2 are clearly asymmetric and drop more sharply on the high energy side.

The Lorentzian broadening parameters Γ are displayed in Fig. 8. The three structures are seen to be broader in HgTe than in CdTe by a factor of ~1.5. The broadening of the $E_1+\Delta_1$ is always larger than that of E_1, as in other semiconducting alloys.[39,40] An asymmetric composition dependence of the broadening is found, it peaks at a composition between x=0.7 and 0.8. This asymmetry can be explained on the basis of the CPA calculations of Ref.37. The conduction band along Λ is broadened about 3 times more efficiently by the disorder on the CdTe than on the HgTe side of the composition range. This is maybe due to the fact that in the CdTe-rich end the final state for the E_1 and $E_1+\Delta_1$ CP's falls in an energy region where HgTe also has a large density of states. The opposite is true for the HgTe-rich end. The conspicuous behavior of the broadening of E_2 is probably due to the existence of several critical points in its energy region.[33]

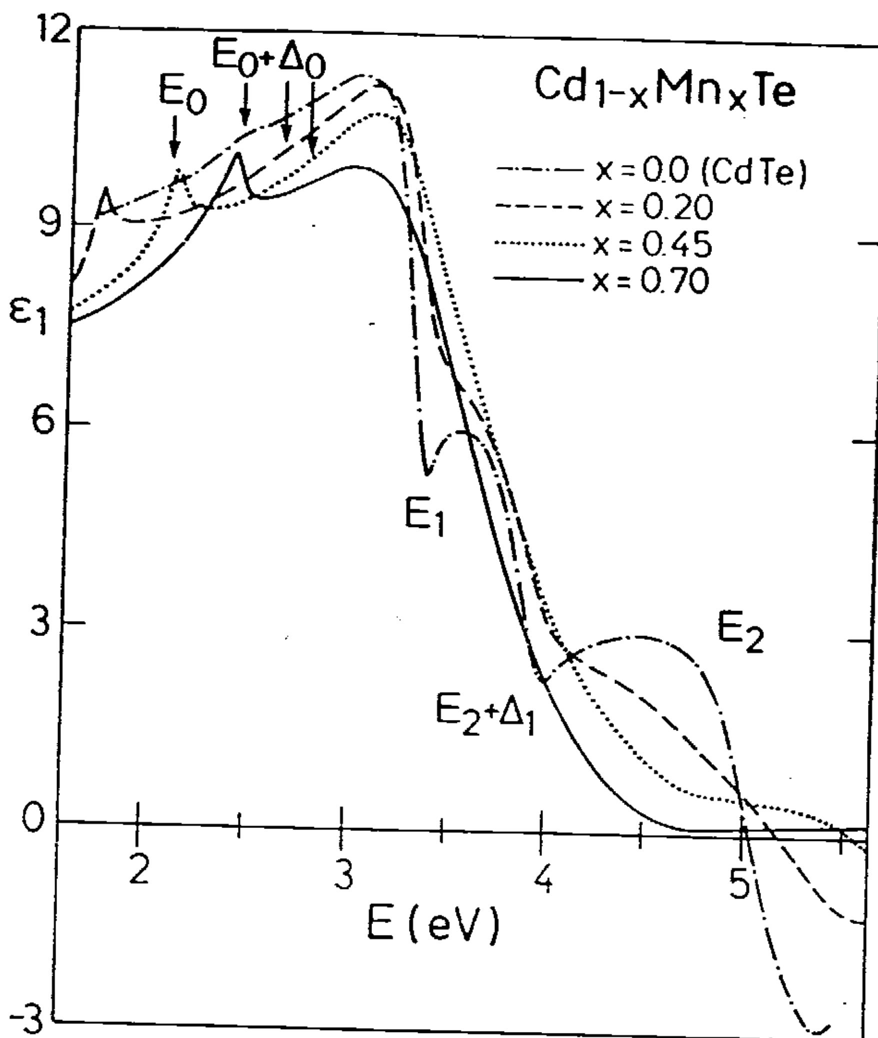

Figure 9.- Real part of the dielectric function of $Cd_{1-x}Mn_xTe$ for different alloy compositions.

The substitution of the Cd element in CdTe by the magnetic transition-metal Mn leads to the class of ternary compounds known as diluted magnetic semiconductors. They crystallize in the zinc-blende structure up to a Mn composition of x=0.7. This alloys show a giant Zeeman splitting of the bands in external magnetic fields,[41] as a result of the exchange interaction between the localized $3d^5$ electrons of the Mn^{+2}-ions and itinerant band electrons.[42] Figure 9 shows the real part of the dielectric function for CdTe and three different alloys. Four structures can be recognized in the spectra: E_0, E_1, $E_1+\Delta_1$ and E_2. A small shoulder corresponding to the $E_0+\Delta_0$ CP at ~2.5 eV can be seen also for CdTe. The E_0 (which is not observed for CdTe) shifts to higher energies with increasing x. The structures related to E_1 and $E_1+\Delta_1$ do not shift noticeable with x, but become much broader and hard to distinguish. The E_2 CP decreases and shifts to higher energies with increasing x and finally moves out of the spectral range. The small red shift of E_1 and $E_1+\Delta_1$ CP's can be qualitatively explained by the interaction of the $L_{4,5}$ states with the Mn dl levels.[36] In contrast with the $Cd_xHg_{1-x}Te$ system, the broadening parameters of the E_1 and $E_1+\Delta_1$ CP's are found to increase linearly with the Mn composition. This is again probably due to the repulsion of the $L_{4,5}$- L_6 valence by the 3d states., which should inhomogeneously broaden these transitions.[36]

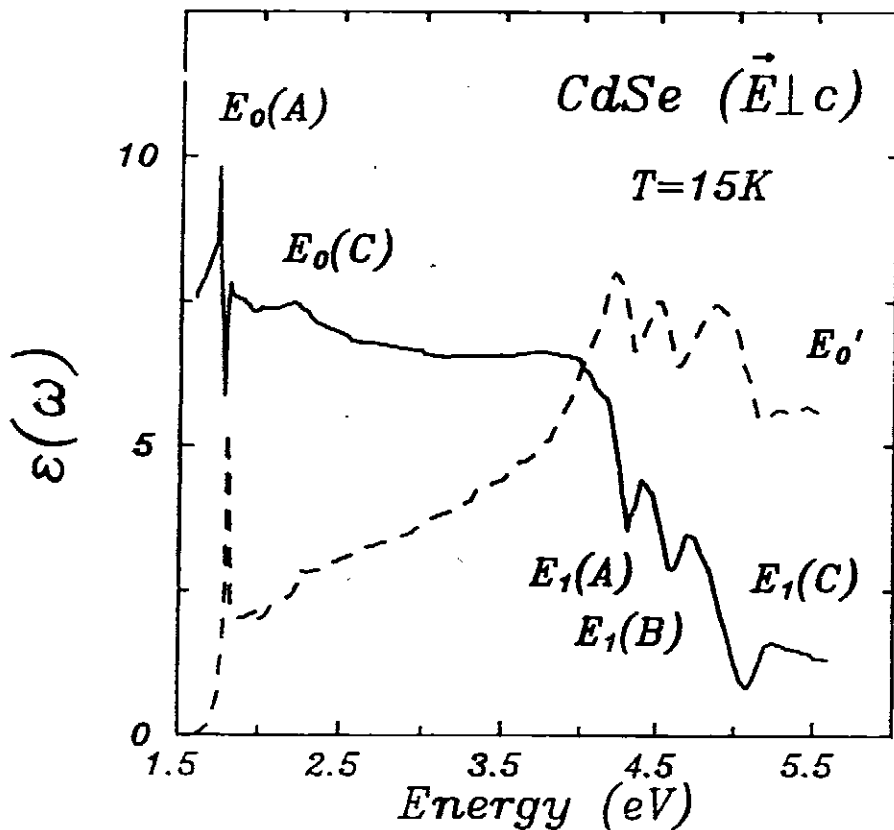

Figure 10.- Dielectric function of CdSe for the ordinary polarization, after Ref. 43.

CdSe is a prototype of a tetrahedral semiconductor, with the hexagonal wurtzite structure. Its optical constants have been investigated in the past by means of transmission and reflectance measurements.[43] The absorption edge (around 2eV) exhibits three excitonic transitions, labeled A (related to a valence band of Γ_9 symmetry), B (Γ_7) and C (Γ_7). The latter structures are observed for both, ordinary (E ⊥ c) and extraordinary (E ∥ c) polarizations, while the former is observed only for E ⊥ c. The A and B excitons, which would be degenerate in a zinc-blende crystal, are split by the hexagonal crystal field, while the spin-orbit interaction at the top of the valence band is responsible for the splitting of the exciton C. We show in Fig. 10 the dielectric function of CdSe, for E ⊥ c, obtained at 15 K. The structure in the 4-5.5 eV region corresponds to the E_1 and $E_1+\Delta_1$ transitions of the zinc-blende materials, except for the existence of strong polarization effects. For E ∥ c only one peak is seen in this region, while three are present for E ⊥ c. The structures can be assigned to direct interband transitions modified by excitonic interaction. By comparison with band structure calculations,[44] the first two peaks observed for E ⊥ c correspond to transitions along the Γ-Δ-A direction between the spin-orbit split Γ_5 and Γ_3 bands. The origin of the additional peak at 5eV for E ⊥ c and E ∥ c lies in transitions along the lateral faces of the Brillouin Zone (BZ), mainly from the M-U-L line, which joins the M and L points on the side faces of the BZ. The edge exciton line-shapes could be fitted with Lorentzian functions at low temperatures, including a dead-layer, however the ϵ_2 line shape transform into a step function as the temperature is increased.[43] The E_1 CP experience a large red shift with increasing temperature, which seems to be characteristic of the wurtzite structure.

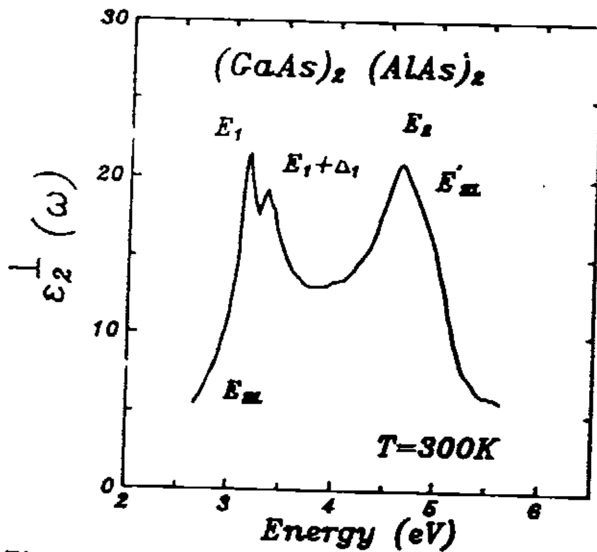

Figure 11.- Imaginary part of the dielectric function of a two-monolayers GaAs/AlAs superlattice, after Ref. 45.

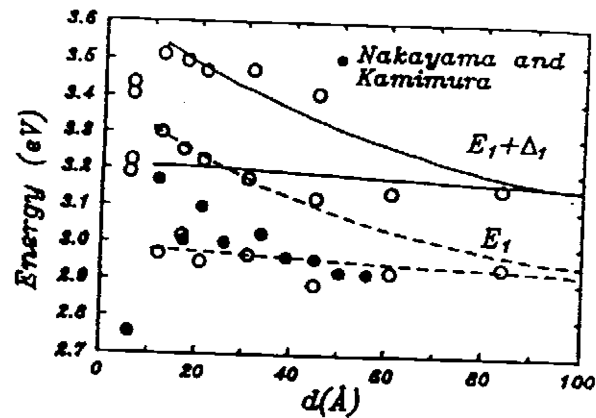

Figure 12.- Dependence of CP energies in GaAs/AlAs superlattices on the period of the SL, after Ref. 46.

5. ELLIPSOMETRY OF LOW DIMENSIONAL SYSTEMS

New optical properties in semiconductors can be obtained taking advantage of the new periodicity attained with superlattices. Their spectra are dominated by excitonic structures close to the main band gap. They also offer possibilities to build new optoelectronic devices since their optical properties can be tailored by band-gap engineering. In (001)-$(GaAs)_m(AlAs)_n$ SL's the main changes in the optical properties are due to the effects of zone-folded bands and to the confinement of the electronic states. Since the relative differences in the band structure of bulk AlAs and GaAs decrease with increasing energy, and because the effective masses become larger, quantum confinement effects for the higher interband transitions appear at thinner SL's periods than for the E_0 gap.

Figure 11 depicts the imaginary part of the dielectric function for a SL with two monolayers of GaAs and AlAs, obtained for incident light perpendicular to the layers using a two-phase model. This model is not strictly valid, but using it a pseudo-ϵ is obtained, which can be interpreted as an average ϵ of the SL, provided that the period is much smaller than the wavelength of the light. The SL spectra contain few extra peaks: a E_{SL} shoulder below E_1, induced by the tetragonal symmetry for SL's where at least one of the constituents layers is wider than one monolayer. This structure has been attributed to transitions near the point where the Γ-L direction cuts the surface of the tetragonal SL BZ.[45] A E'_{SL} shoulder, with similar origin as the E_2 structure in bulk zinc-blende compounds, arises from parallel-bands transitions along the Γ-X direction and transitions between folded bands near Γ-Z. The assignment is made based on calculations performed with the self-consistent scalar relativistic linear muffin-tin-orbital method together with the local-density-approximation formalism.[45]

For periods smaller than 50A a splitting of E_1 and $E_1+\Delta_1$ is observed,[46] as shown in Fig. 12, while no noticeable effects are seen for E_2. For large periods (d>50A) the confinement of the electronic states in the GaAs wells shifts slightly the E_1 and $E_1+\Delta_1$ transitions towards the blue.

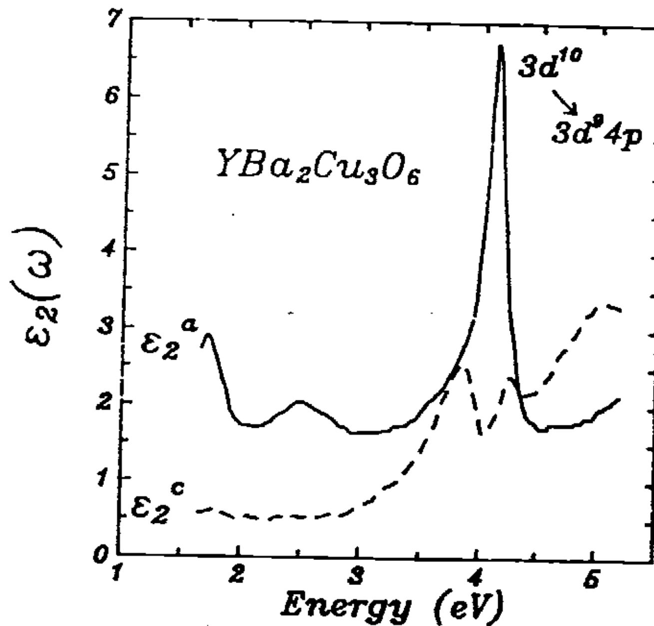

Figure 13.- Imaginary part of the dielectric function of $YBa_2Cu_3O_6$ perpendicular to the c axis (ϵ^a) and along the c axis (ϵ^c), after Ref. 48.

6. NEW DEVELOPMENTS

We will review briefly in this section new results obtained by ellipsometry in Y-Ba-Cu-O compounds and the extension of the spectral range towards the ultra-violet region. The optical spectra of high T_c superconductors have been studied primarily in the infrared region, in order to investigate excitations that are possibly involved in the phenomenon of superconductivity. The electronic transitions at higher energies provide an insight into the electronic structure of the normal states, that can be compared with band structure calculations. In $YBa_2Cu_3O_7$ three major structures have been observed in the spectra: one centered at ~2.8 eV, which corresponds to interband transitions within hybridized O(2p)-Cu(3d) states, and two structures at 4.1 and 4.7 eV within O(2p)-Ba(5d) states.[47]

Removal of oxygen from the high T_c superconductor causes the compound to be a semiconductor rather than a superconducting metal. In the superconductor ϵ_2 is flat with weak structures at 2.8 and 4.7eV.[47] Decreasing the oxygen content three new features appear in the spectra. There is a controversy in the literature about the origin of the 4eV peak, which is either related to the existence of a O(IV)-Cu(I)-O(IV) complex or to a O-Ba transition.[48] The investigation of the anisotropy of ϵ in single crystals gives additional information to clarify the origin of the peak. Figure 13 shows the imaginary part of the dielectric function for $YBa_2Cu_3O_6$ perpendicular to the c axis (ϵ^a, with polarization in the ab plane of the crystal) and along the c axis (ϵ^c).[48]

Self-consistent band-structure calculations using the spin-restricted local-density approximation were used to interpret the data, neglecting excitonic interactions.[48] According to the calculations the 4eV peaks arise from initial- and final-states bands which are nearly parallel near the boundary of the tetragonal BZ. It is mainly related to intraionic $3d^{10}$- $3d^9 4p$ transitions in the Cu ion of the O-Cu-O dumbbell, with small contributions from the Cu-Ba charge-transfer transitions. The initial- and final-states wavefunctions are located in the O-Cu-O dumbbells and in the BaO-Cu-OBa triple layer.

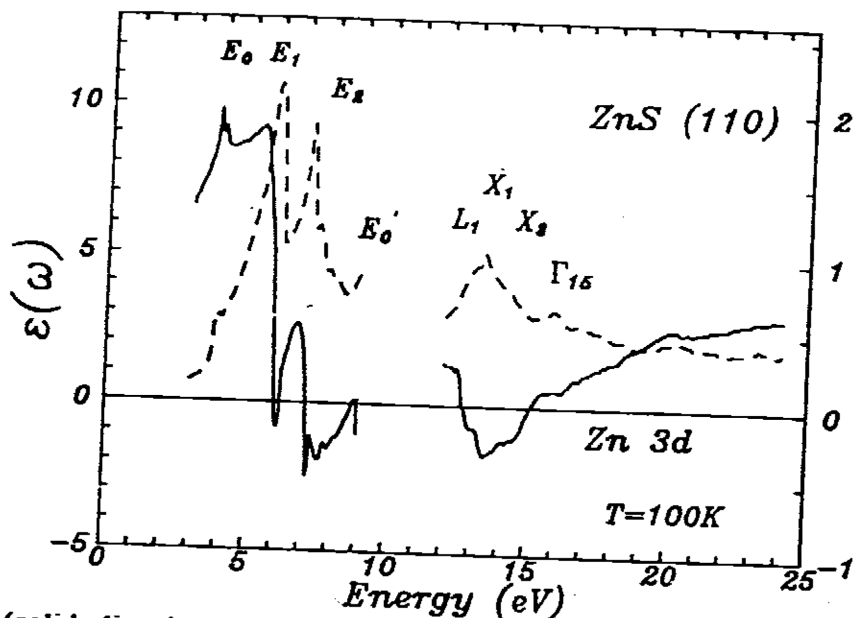

Figure 14.- Real (solid lines) and imaginary (dashed lines) part of the dielectric function of ZnS at 100K obtained with synchrotron radiation light, after Ref. 49.

Finally, we show in Fig. 14 the real (solid lines) and imaginary (dashed lines) parts of the dielectric function of a (110) ZnS sample at 100K, obtained at the synchrotron radiation facility BESSY.[49] The reflected light was analyzed by a rotating triple-reflection polarizer, and the measurements were performed under UHV conditions (10^{-9} mbar). Below 10 eV the usual electronic interband transitions are observed, which show a strong excitonic character. Of particular interest are the regions around the anion core thresholds, Zn 3d, which are beyond the range of conventional ellipsometry. The assignment of the structures was made by comparison with relativistic linear-muffin-tin-orbital calculations.

7. ACKNOWLEDGMENTS

Most of this work was performed at the Max-Planck-Institut für Festkörperforshung (Stuttgart, F.R.G.) with strong collaboration with P. Lautenschlager, S. Logothetidis, and C. Umbach. We would also like to thank H. Hirt, M. Siemers, and P. Wurtser for expert technical help, M. Bleder and A. Birkner for help with the construction of the ellipsometer, and F. Calle for a careful reading of the manuscript. One of the authors (L.V.) wish also to thank the Spanish Ministery of Education for partial finance of this work under the Project No. MAT-88-0116-C02-02.

8. REFERENCES

1. See, for example, R.M.A. Azzam and N.M. Bashara, *Ellipsometry and Polarized Light* (North-Holland, Amsterdam, 1977).
2. D.E. Aspnes, J. Opt. Soc. Am. 64, 812 (1974).
3. D.E. Aspnes, Opt. Commun. 8, 222 (1973).
4. D.E. Aspnes and A.A. Studna Applied Optics 14, 220 (1975)
5. D.E. Aspnes, J. Vac. Sci. Technol. 17, 1067 (1980); Appl. Phys. Lett. 39, 316 (1981).)
6. L. Viña and M. Cardona, Phys. Rev. B 29, 6739 (1984).
7. P. Lautenschlager, P.B. Allen and M. Cardona, Phys. Rev. B 31, 2163 (1985).)

8. L. Viña and M. Cardona, Phys. Rev. B 34, 2586 (1986).
9. S. Logothetidis, M. Cardona, P. Lautenschlager and M. Garriga, Phys. Rev. B 34, 2458 (1986).
10. S. Logothetidis, L. Viña and M. Cardona, Phys. Rev. B 31, 2180 (1985).
11. See, for example, specially issue of IEEE J. Quant. Elect., QE-22, (1986).
12. F.H. Pollak and O.J. Glembocki, in *Proceddings of the Society of Photo-Optical Instrumentation Engineers*, (SPIE, Bellingham 1988), 946, 2 (1988).
13. F.H. Pollak and H. Shen, Superl. and Microst. 6, 203 (1989).
14. B.V. Shanabrook, O.J. Glembocki, D.A. Broido, L. Viña and W.I. Wang, J. de Physique C5, 48, 235 (1987).
15. M. Alouani, S. Gopalan, M. Garriga, and N.E. Christensen, Phys. Rev. Lett. 61, 1643 (1988).
16. M. Garriga, M. Cardona, N. E. Christensen, P. Lautenschlager, T.Isu and K. Ploog, Phys. Rev. B 36, 3254 (1987).
17. J. Barth, R.L. Johnson, M. Cardona, D. Fuchs and A.M. Bradshaw in *Proc. 19th Int. Conf. Phys. Semic.*, Warsaw, 1988. Edited by W. Zawadski. Institute of Physics, Polish Academy of Sciences (1988), p. 885.
18. A. Compaan and H.J. Trodahl, Phys. Rev. B 29, 793 (1984).
19. G.E. Jellison, Jr., D.H. Lowndes and R.F. Wood, Phys. Rev. B 28, 3272 (1983).
20. P.B. Allen and M. Cardona, Phys. Rev. B 27, 4760 (1983), and references therein.
21. L. Viña, S. Logothetidis, and M. Cardona, Phys. Rev. B 30, 1979 (1984).
22. P. Lautenschlager, P.B. Allen, and M. Cardona Phys. Rev. B 33, 5501 (1986).
23. L. Viña, H. Höchst, and M. Cardona, Phys. Rev. B 31, 958 (1985).
24. S. Logothetidis, L. Viña, and M. Cardona, Phys. Rev. B 31, 947 (1985).
25. P. Lautenschlager, M. Garriga, S. Logothetidis, and M. Cardona, Phys. Rev. B 35, 9174 (1987).
26. S. Gopalan, P. Lautenshlager, and M. Cardona, Phys. Rev. B 35, 5577 (1985).
27. P. Lautenshlager, M. Garriga, L. Viña, and M. Cardona, Phys. Rev. B 36, 4821 (1987).
28. J.E. Rowe and D.E. Aspnes, Phys. Rev. Lett. 25, 162 (1970).
29. Y.P Varshni, Physica (Utrecht) 34, 149 (1967).
30. See references 6 and 8, and references therein.
31. D.E. Aspnes, A.A. Studna and E. Kinsbron, Phys. Rev. B 29, 768 (1984).
32. G.E. Jellison, Jr., F.A. Modine, C.W. White, R.F. Wood and R.T. Young, Phys. Rev. Lett. 46, 1414 (1981).
33. L. Viña, C. Umbach, M. Cardona, and L. Vodopyanov, Phys. Rev. B 29, 6752 (1984).
34. K. Kumazaki, L. Viña, C. Umbach, and M. Cardona, Solid State Commun. 68, 591 (1988).
35. K. Kumazaki, L. Viña, C. Umbach, and M. Cardona, Physica Stat. Solidi (b) 156, 371 (1989).
36. P. Lautenschlager, S. Logothetidis, L. Viña, and M. Cardona Phys. Rev. B 32, 3811 (1985).
37. K.C. Haas, H. Ehrenreich and B. Velicky, Phys. Rev. B 27, 1088 (1983).
38. D.J. Chadi, Phys. Rev. B 16, 790 (1977).
39. P. Parayanthal, C.S. Ro, F.H. Pollak, C.R. Stanley, G.W. Wicks, and L.F. Eastman, Appl. Phys. Lett. 43, 109 (1983).
40. S.M. Kelso, D.E. Aspnes, M.A. Pollak, and R.E. Nahory, Phys. Rev. B 26, 6669 (1982).
41. D.L. Peterson, A. Petrou, M. Datta, A.K. Ramdas, and S. Rodriguez, Solid State Commun. 43, 667 (1982).
42. N.B. Brandt and V.V. Moshchalkov in *Advances in Physics* 33, 193 (1984)
43. See, S. Logothetidis, M. Cardona, P. Lautenschlager and M. Garriga, Phys. Rev. B 34, 2458 (1986), and references therein.
44. A. Kobayashi, O.F. Sankey, and S.M. Volz, Phys. Rev. B 28, 935 (1983).
45. M. Alouani, S. Gopalan, M. Garriga, and N.E. Christensen, Phys. Rev. Lett. 61, 1643 (1988).

46. M. Garriga, M. Cardona, N. E. Christensen, P. Lautenschlager, T.Isu and K. Ploog, Phys. Rev. B 36, 3254 (1987).
47. J. Humlicek, M. Garriga, M. Cardona, B. Gegenheimer, E. Schönherr, P. Beberich and J. tate, Solid State Commun. 66, 1071 (1988).
48. See, J. Kircher, M. Alouani, M. Garriga, P. Murugaraj, J. Maier, C. Thomsen, M. Cardona, O.K. Andersen and O. Jepsen, Phys. Rev. B 40, 7368 (1989).
49. J. Barth, R.L Johnson, M. Cardona, D. Fuchs and A.M. Bradshaw in *Proceedings of the 19th International Conference on the Physics of Semiconductors*, edited by W. Zawadzki (Institute of Physics, Polish Academy of Sciences, Warsaw 1988), p. 885.